Photoreversal Kinetics of the I_1 and I_2 Intermediates in the Photocycle of Photoactive Yellow Protein by Double Flash Experiments with Variable Time Delay†

Chandra P. Joshi,‡ Berthold Borucki,‡ Harald Otto,‡ Terry E. Meyer,§ Michael A. Cusanovich,§ and Maarten P. Heyn*,‡

Biophysics Group, Physics Department, Freie Universität Berlin, Arnimallee 14, D-14195 Berlin, Germany, and Department of Biochemistry and Molecular Biophysics, University of Arizona, Tucson, Arizona 85721

Received September 1, 2004; Revised Manuscript Received October 28, 2004

ABSTRACT: We investigated the kinetics of photoreversal from the I_1 and I_2 intermediates of photoactive yellow protein (PYP) by time-resolved optical absorption spectroscopy with double flash excitation. A first flash, at 430 nm, initiated the photocycle. After a variable time delay, the I_1 intermediate was photoreversed by a second flash, at 500 nm, or a mixture of I_2 and I_2' intermediates was photoreversed by a second flash, at 355 nm. By varying the delay from 1 μs to 3 s, we were able to selectively excite the intermediates I_1, I_2, and I_2'. The photoreversal kinetics of I_2 and I_2' at 21 different delays and two wavelengths (340 and 450 nm) required two exponentials for a global fit with time constants of $\tau_1 = 57 \pm 5$ μs and $\tau_2 = 380 \pm 40$ μs (pH 6, 20 °C). These were assigned to photoreversal from sequential I_2 and I_2' intermediates, respectively. The good agreement of the delay dependence of the two amplitudes, A_1 and A_2, with the time dependence of the I_2 and I_2' populations provided strong evidence for the sequential model. The persistence of A_1 beyond delay times of 5 ms and its decay, together with A_2 around 500 ms, suggest moreover that I_2 and I_2' are in thermal equilibrium. The wavelength dependence of the photoreversal kinetics was measured at 26 wavelengths from 510 to 330 nm at the two fixed delays of 1 and 10 ms. These data also required two exponentials for a global fit with $\tau_1 = 59 \pm 5$ μs and $\tau_2 = 400 \pm 40$ μs, in good agreement with the delay results. Photoreversal from I_2' is slower than from I_2, since, in addition to chromophore protonation, the global conformational change has to be reversed. Our data thus provide a first estimate of about 59 μs for deprotonation and 400 μs for the structural change, which also occurs in the thermal decay of the signaling state but is obscured there since reisomerization is rate-limiting. The first step in photoreversal is rapid *cis*−*trans* isomerization of the chromophore, which we could not resolve, but which was detected by the instantaneous increase in absorbance between 330 and 380 nm. In agreement with this observation, the spectrum of the $I_2'^{trans}$ intermediate, derived from the A_2 amplitude spectrum, has a much larger extinction coefficient than the spectrum of the $I_2'^{cis}$ intermediate. With a first flash, at 430 nm, and a second flash, at 500 nm, we observed efficient photoreversal of the I_1 intermediate at a delay of 20 μs when most molecules in the cycle are in I_1. We conclude that each of the three intermediates studied can be reversed by a laser flash. Depending on the progression of the photocycle, reversal becomes slower with the time delay, thus mirroring the individual steps of the forward photocycle.

Photoreceptors with photoisomerizable double bonds in their chromophores have numerous features in common. One of these is that many photointermediates, in particular the signaling state, can be reversed by light directly back to the initial dark state. This process is called photoreversal. Photoreceptors with this property are called photochromic: they can be switched back and forth by light between the inactive dark and active signaling states. Photoreversible reactions play a key role in signal transduction. Examples of photochromic photoreceptors are rhodopsin (*1*, *2*), phytochrome (*3*, *4*), sensory rhodopsin I (*5*), and photoactive yellow protein (PYP).[1] Growth and development of plants are controlled by photoreversible reactions between two interconvertible species of phytochrome, P_r and P_{fr}. The biological significance of the control by light of the switching between the P_r and P_{fr} forms is well documented (*3*, *4*). In SR-I from *Halobacterium salinarium* the dark form SR_{587} is an attractant receptor while its long-lived photointermediate SR_{373} mediates repellent taxis by blue light. The color-discriminating phototaxis keeps the cells in the optimal spectral range for energy transduction, while avoiding damage by UV light. The light-driven proton pump bacteriorhodopsin can also be photoreversed from its bleached

† C.P.J. was supported by a fellowship from the DFG (GRK 788, project A9, grant to M.P.H.). This work was also supported in part by NIH Grant GM 66146 to M.A.C.

* Corresponding author. E-mail: heyn@physik.fu-berlin.de. Fax: +49-30-8385 6299. Phone: +49-30-8385 6160.

‡ Freie Universität Berlin.

§ University of Arizona.

[1] Abbreviations: PYP, photoactive yellow protein; PAS, acronym formed from the names of the first three proteins recognized as sharing this sensory domain.

10.1021/bi0481141 CCC: $30.25
Published on Web 12/22/2004

state M (*6*). In the case of invertebrate rhodopsin, the visual cycle is a two quantum process, and the photoreversal from the M intermediate constitutes the basis for light adaptation (*2*). For *Halorhodospira halophila* PYP, the biological significance of the photochromicity has not yet been investigated in detail at the cellular level, although in *Rhodocista centenum* Ppr, a kinase activity and thus gene regulation is modulated by light (*7*). In addition to its intrinsic biological significance, this photochromic molecular switching property is of potential technological interest in the development of optical storage and switching devices.

Photoactive yellow protein (PYP) is a photoreceptor protein that was originally discovered in *H. halophila* (for recent reviews see refs *8* and *9*). Seven species of PYP have been identified to date (*10*). In *Rc. centenum* Ppr, PYP is associated with bacteriophytochrome and histidine kinase domains, which are involved in regulation of a polyketide synthase gene (*7*). Whereas the function of PYP was long believed to be as a blue light receptor for negative phototaxis in *H. halophila*, there are recent suggestions that other species of PYP may be involved in controlling cell buoyancy through regulation of gas vesicle genes (*10*). PYP is the prototype of a structural motif termed PAS domain, which is found in a large and widely distributed class of sensory proteins that respond to a diverse range of compounds and stimuli (for example, light, oxygen, small organics, and electric fields) (*8*, *10*−*12*).

PYP is a suitable model system to study signal transduction, since high-resolution structures are available for the dark state and some of the photocycle intermediates (*13*−*16*). PYP has a 4-hydroxycinnamoyl chromophore that is bound via a thioester linkage to cysteine 69. It is anchored in its binding pocket by three hydrogen bonds. Two of these hydrogen bonds are between the chromophore hydroxyl group and glutamate 46 and tyrosine 42. The third is between the chromophore carbonyl and the amide proton of cysteine 69. In the dark state, the chromophore hydroxyl is deprotonated, and the absorption maximum of the chromophore is at 446 nm. Electronic excitation leads to rapid isomerization around the C_7═C_8 double bond. Upon isomerization, the hydrogen bonds with E46 and Y42 remain intact, but the thioester part of the chromophore, including the carbonyl, flips ∼180° forming a transient intermediate termed I_1 in ∼3 ns. An essential step in formation of the signaling state is the protonation of the chromophore and a subsequent global conformational change. Evidence from time-resolved FTIR (*17*, *18*), flash spectroscopy (*19*, *20*), and transient dye binding (*19*, *21*) suggests that there are at least two intermediates with protonated chromophores, termed I_2 and I_2'. I_2 is formed in approximately 300 μs, and subsequently I_2' is formed in ∼3 ms and decays to the ground state in hundreds of milliseconds. Both I_2 and I_2' have absorption spectra with maxima at ∼350 nm, with a major global conformational change occurring when I_2' is formed in which a hydrophobic surface area is exposed (*22*). Thus I_2' is presumably the long-lived signaling state to which an unknown response regulator binds. Several models have been proposed for the mechanism of conformational change. In the "protein quake model" (*17*), the conformational change is triggered electrostatically by proton transfer from E46 to the chromophore. In the "hydrophobic collapse model" (*8*), the movement of the chromophore out of its binding pocket leads to the collapse of the hydrophobic residues lining the binding pocket. The resulting strain on one side of the central β-sheet is transmitted to the other side, leading to a conformational change in the N-terminal domain (*8*). It is important to understand the mechanism of this long-range activation process from the chromophore binding pocket to the N-terminal domain.

The initial evidence for photoreversals in PYP came from kinetic experiments with a photostationary mixture of I_2 and the ground state in wild type (*23*, *24*) and in the mutant M100A, which has a long-lived I_2 intermediate (*25*). By lowering the pH to 5.6 and using background light, approximately 70% of the PYP molecules could be accumulated in the I_2 state of the wild-type PYP (*24*). Transient absorption measurements with excitation at 355 nm and nanosecond time resolution showed that rapid unresolved photoisomerization occurred, converting I_2 (which is the *cis* isomer) to an I_2^{trans} form. I_2^{trans} then decayed monoexponentially to the initial dark state (P) with an exponential time constant of 147 μs at room temperature (*24*). Compared to the thermal decay, the light-induced decay of I_2 in wild-type PYP is approximately 10^3 times faster. In the mutant M100A, the lifetime of I_2 is in the minutes range, allowing almost 100% accumulation of I_2 after illumination (*25*). The return to P via the photo-back-reaction from I_2 in this mutant was also monoexponential with a time constant of 230 μs (*25*).

In previous work with wild-type PYP, the photoreversal from I_2 was induced in a photo steady state with a mixture of I_2 and I_2' intermediates of unknown composition. Whereas in the photo-back-reaction from I_2 the isomerization and chromophore protonation have to be reversed, in the photo-back-reaction from I_2', the global conformational change has to be reversed in addition. It thus seems likely that the kinetics of the photoreversal will differ between I_2 and I_2'. Here, we perform double flash experiments to differentiate between the photoreversal kinetics of I_2 and I_2'. A first flash, at 430 nm, initiates the photocycle. After a variable time delay (from 1 μs to 3 s), a second flash, at 355 nm, photoreverses I_2. By varying the delay, we can selectively excite I_2 or I_2'. In this way, we are able to show that the kinetics depends on the delay and have different rate constants for I_2 and I_2'. By using a second flash, at 500 nm, and a shorter delay of 20 μs, we could selectively excite I_1 and demonstrate for the first time photoreversal from this earlier intermediate as well.

MATERIALS AND METHODS

PYP from *H. halophila* was prepared as previously described (*22*), and kinetic experiments were carried out in a buffer consisting of 20 mM Tris and 50 mM KCl at pH 6 and 20 °C.

Time-resolved absorption spectroscopy with single and double flash excitation was performed as described (*6*, *26*, *27*). For the photoreversal experiments on I_2, the first flash at 430 nm (intensity 10 mJ/cm^2) is from an excimer pumped dye laser (10 ns) using the laser dye Stilbene 3. The second flash at 355 nm (intensity 10 mJ/cm^2) was from a frequency-tripled Nd:YAG laser (10 ns). For the photoreversal experiments on I_1, the second flash at 500 nm (intensity 10 mJ/cm^2) was from an excimer pumped dye laser (10 ns) using

the laser dye coumarin 307. The samples were measured in a 5 × 5 mm quartz cuvette. The OD of the sample was 1.43 at 446 nm. The directions of the two flash excitation beams were perpendicular to that of the measuring beam. The light source in the measuring beam was a 100 W tungsten−halogen lamp providing an intensity of 100 μW/cm^2 at 450 nm at the sample after the first monochromator. Attenuation of the intensity of the measuring beam had no effect on the observed kinetics, suggesting that the intensity was small enough to avoid the buildup of photostationary states. The spectral bandwidth of the monochromators in the measuring beam was ±4 nm. A homemade generator allowed delays to be set between the two laser pulses from 1 μs to 3 s with an accuracy of 100 ns. The delay was checked with a counter. Data acquisition, signal processing, and digitalization were performed as described previously (*6*, *26*) with two overlapping channels with different sampling rates. The first channel was measured with a 1 GHz sampling oscilloscope (8 bit) and the second channel with a fast A/D converter (12 bit). The data acquisition was triggered either on the first or on the second flash. The data were compressed and averaged by changing from the linear to a logarithmic time scale (*26*). The reduced data sets consist of 100 data points per time decade. As a consequence of this data acquisition method, the signal to noise ratio increases with the time after the flash (see, for example, data of Figure 3A). This effect was taken into account in the data analysis by using appropriate weighting factors which increased the weight of the later data points.

RESULTS

Construction of the Photoreversal Signal from I_2. Typical transient absorption data for the photoreversal reaction from I_2 at 340 and 450 nm are shown in panels A and B of Figure 1. The delay between the two flashes was 10 ms as indicated by the arrows. At this time, most molecules cycling are in the I_2' intermediate state. Panel C of Figure 1 shows the absorption spectra of the three states P, I_1, and the I_2/I_2' equilibrium with vertical lines marking the wavelengths of the two flashes. Panels A and B of Figure 1 each contain six time traces labeled BFTB, DFTB, DFTV, BFTV, VFTV, and PR (photoreversal signal). The first five traces are the data. The photoreversal signal was constructed from the traces DFTV, BFTV, and VFTV as follows. The trace BFTB (black) is the normal single flash trace: *b*lue *f*lash (430 nm) *t*riggered on *b*lue flash. The absorbance increase at 340 nm about 300 μs after excitation is due to the formation of I_2 (Figure 1A). The corresponding kinetic component in the ground-state depletion signal is the absorbance decrease at 450 nm due to the I_1 to I_2 transition (Figure 1B). The photoreversal reaction is evident from the traces labeled DFTB (red) in panels A and B of Figure 1. DFTB stands for *d*ouble *f*lash *t*riggered on the *b*lue flash. At 340 nm (Figure 1A) there is a positive spike followed by a large unresolved drop in absorbance at the delay time of 10 ms (marked by arrow). At 450 nm (Figure 1B), there is a large unresolved increase in absorbance. Together, these effects are the signature of photoreversal from I_2/I_2' to P: the concentration of I_2/I_2' (absorbing around 350 nm) drops and simultaneously the concentration of the initial dark state P (absorbing around 450 nm) increases. The kinetics of the photo-back-reaction is clearly fast compared to the I_2 to I_2' transition and cannot be resolved by using a logarithmic time base when triggering on the first (blue) flash. The photoreversal from I_2 can be resolved, however, by triggering on the second (violet, 355 nm) flash. This is shown in the traces labeled DFTV (green) in panels A and B of Figure 1: *d*ouble *f*lash *t*riggered on the *v*iolet flash. Note that when the trigger is on the second flash, the zero of the time basis (origin of the horizontal axis of Figure 1A,B) is the second flash.

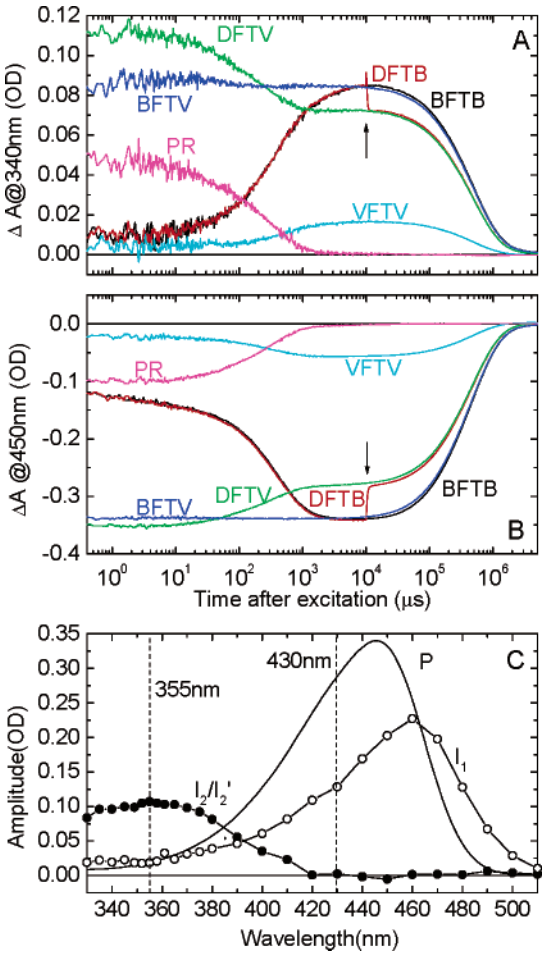

FIGURE 1: Absorbance changes at 340 nm (A) and 450 nm (B) after single (430 or 355 nm) or double flash excitation [430 nm followed by 355 nm 10 ms later (arrow)]. Each trace is the average of 10 flashes. Note the logarithmic time scale. The double flash traces labeled DFTB and DFTV are triggered on the first flash (430 nm) and on the second flash (355 nm), respectively. If the trigger is on the second flash, that flash sets the zero time point on the horizontal time axis. Single flash signals with either blue (B, 430 nm) or violet (V, 355 nm) excitation and triggered on the first (BFTB) or second flash (BFTV, VFTV) are displayed as well. These are needed to construct the photoreversal signal (PR) according to eq 2, with $f_1 = 0.76$ and $f_2 = 0.73$. Conditions: pH 6, 20 °C, 20 mM Tris, and 50 mM KCl. (C) Absorption spectra of P, I_1, and the I_2/I_2' equilibrium mixture, together with markers indicating the wavelengths of the blue (430 nm) and violet (355 nm) flashes. The spectra of the I_1 intermediate and the I_2/I_2' equilibrium mixture were calculated from the single flash data of Figure 4B as described in the text.

At the time of the second flash, there exists a mixed population of the intermediates I_1, I_2, and I_2' as well as the remaining population of PYP molecules that were not excited by the first flash. The violet flash is able to excite all of these species (see overlapping intermediate spectra in panel C of Figure 1; these spectra were calculated from the data of Figure 4B, as described below). Except for the very short

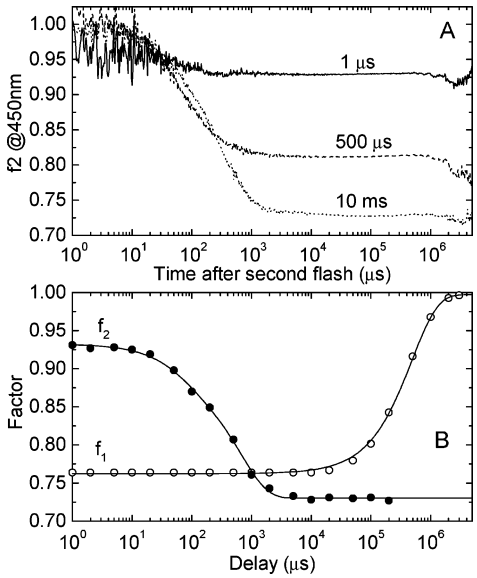

FIGURE 2: (A) Correction factor $f_2(t)$ calculated according to eq 1 for delays of 1 μs, 500 μs, and 10 ms. The plateau values are plotted in panel B for various delays. (B) Correction factors f_1 and f_2 for various values of the time delay between the flashes. f_1 is the fraction of PYP molecules not excited by the first flash. f_2 is the fraction of cycling PYP molecules not excited by the second flash.

delays, the photoreversal from I_1 can be ignored (see below). Therefore, we need only to correct for the fraction of PYP molecules that were not excited by the first, blue flash but were excited by the second, violet flash. The traces labeled VFTV, *v*iolet *f*lash triggered on the *v*iolet *f*lash, show that the excitation of the PYP sample by a single flash, at 355 nm, is quite efficient. Moreover, these traces have the same kinetics as for excitation at 430 nm and contribute in the same time range as the photoreversal changes (compare DFTV with VFTV). Thus, the double flash signal DFTV has to be corrected for the contribution from those molecules that were not excited by the first, blue flash but by the second, violet flash. To make this correction, we need to know f_1, the fraction of the initial PYP population that was not excited by the first flash and remains in the ground state. Since f_1 equals 1 minus the probability of cycling induced by the first flash, f_1 was determined by measuring the amplitude of the ground-state depletion signal at 450 nm and comparing it with the dark absorption at 450 nm. In this way, typical values for f_1 of 0.76 were obtained. This means that, with our laser system, the first flash drove 24% of the molecules through the photocycle. The remaining 76% could be excited by the second, violet flash. The dependence of f_1 on the delay is shown in Figure 2B. Since no significant thermal relaxation from I_2 back to the ground state occurs up to about 10 ms, f_1 remains constant up to that time (Figure 2B). With delays beyond this value, a growing number of molecules return to the initial state, thus f_1 increases to a final value of 1.

To obtain the true photoreversal signal, the double flash absorption change also has to be corrected for the contribution from the first flash of those molecules in the cycle that are not excited by the second flash and thus complete the thermal cycle. The trace BFTV (*b*lue *f*lash *t*riggered on *v*iolet flash) corresponds to a single blue flash excitation triggered at the time point where the second, violet flash would have occurred in the double flash excitation. This trace has to be weighted by f_2, the fraction of cycling PYP molecules not excited by the second flash. f_2 was determined in a similar way as f_1 from the amplitudes of the depletion signal at 450 nm at times after completion of the photoreversal kinetics. Its calculation is based on the assumption, borne out by the experimental data, that the photoreversal kinetics are faster than the thermal decay of I_2 to P. $f_2(t)$ is defined as the value of the ratio

$$f_2(t) = \frac{\Delta A_{\mathrm{DFTV}}(t) - f_1 \Delta A_{\mathrm{VFTV}}(t)}{\Delta A_{\mathrm{BFTV}}(t)} \quad (1)$$

and evaluated at 450 nm. At times after completion of the photoreversal reaction, the numerator is the amplitude of the depletion signal after photoreversal (DFTV) corrected for the contribution from the molecules that were not excited by the first flash but by the second violet flash (VFTV). The denominator is the amplitude of the depletion signal in the normal single flash photocycle, i.e., in the absence of photoreversal. This ratio is exactly the fraction of molecules cycling that continues along the thermal photocycle after the second flash, i.e., the fraction not excited by the second flash. Using the time traces DFTV, VFTV, and BFTV as well as the value of f_1, $f_2(t)$ was calculated according to eq 1 as a function of time. In Figure 2A $f_2(t)$ is plotted for delays of 1 μs, 500 μs, and 10 ms. At times after completion of the photoreversal reaction ($>\sim$2 ms), $f_2(t)$ reaches a constant time-independent value (see Figure 2A). This constant f_2 is the fraction required and used in eq 2 below. These values depend on the delay (Figure 2A) and are plotted in Figure 2B. At short delays ($<$20 μs), f_2 is not equal to 1 as one might have expected but to $\sim$0.93. This is due to photoreversal from I_1. Evidence for efficient photoreversal from I_1 with a second flash at 500 nm will be presented below. We note that, based on the spectrum of I_1 in Figure 1C, some photoreversal from I_1 with excitation at 355 nm is to be expected. Figure 2B shows that f_2 decreases between delays of 100 μs and 2 ms from about 0.87 to about 0.74. This is due to the growth of the I_2/I_2' population in this time interval. The photoreversal signals ΔA_{PR} (violet traces) shown in Figure 1A,B were obtained from the traces labeled DFTV, VFTV, and BFTV using eq 2 and the delay-dependent correction factors f_1 and f_2 of Figure 2B:

$$\Delta A_{\mathrm{PR}}(t) = \Delta A_{\mathrm{DFTV}}(t) - f_1 \Delta A_{\mathrm{VFTV}}(t) - f_2 \Delta A_{\mathrm{BFTV}}(t) \quad (2)$$

The photoreversal absorbance signals in Figure 1A,B, constructed in this way, are exactly zero after completion of the photoreversal reaction and do not contain any contribution from the single, blue flash photocycle as a consequence of the definition of the correction factor f_2. Thus, the f_2 correction used here greatly simplifies the analysis of the photoreversal kinetics by removing the unrelated kinetic components from the normal photocycle prior to analysis. Comparing the DFTV and PR traces in panels A and B of Figure 1, the effect of corrections is twofold: the f_1 correction has removed the kinetic contributions from the photocycle intermediates formed by the second flash, and the f_2 correction has removed the kinetic contribution from those molecules not excited by the second flash but continuing to P along the normal thermal cycle.

Dependence on Delay. The experiment shown in Figure 1, at a delay of 10 ms, was carried out at 20 additional delays

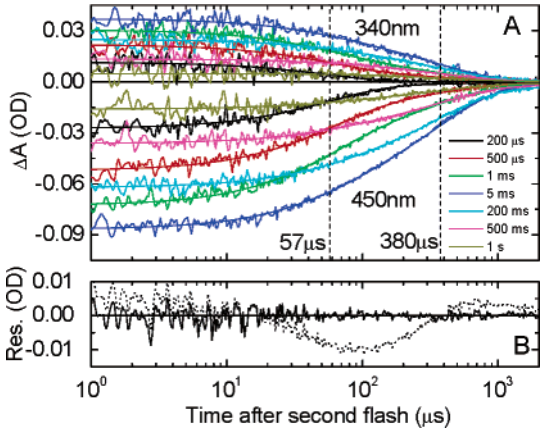

FIGURE 3: (A) Corrected photoreversal signals at 340 and 450 nm at seven delays ranging from 1 μs to 3 s. For clarity, the data at the 14 other delays are not shown. The solid lines represent a two-exponential global fit to all of the data with $\tau_1 = 57$ μs and $\tau_2 = 380$ μs. Conditions: pH 6, 50 mM KCl, 20 °C, and 20 mM Tris. (B) Residuals of the fit to the 450 nm photoreversal signal at a delay of 1 ms. Black dots: one-exponential fit. Black line: two-exponential fit.

ranging from 1 μs to 3 s, at both 340 and 450 nm. The calculated photoreversal signals, positive at 340 nm and negative at 450 nm, were constructed as described above. Of the corresponding 21 traces, for clarity, only 7 are presented at each wavelength in Figure 3A. We note that a number of these traces cross, indicating that they cannot be fitted simultaneously by a single exponential with a common time constant. For a global fit to all data sets, a sum of two exponentials with comparable amplitudes was required. In Figure 3B, we show, as an example, the residuals at 450 nm for a one-exponential and a two-exponential global fit to the data of Figure 3A at a delay of 1 ms. Systematic deviations are apparent in the residuals for the one-exponential fit, while residuals for the two-exponential fit appear to be randomly distributed around zero. The complete set of data at the 2 wavelengths and 21 delays could be fitted with two exponentials with the common time constants $\tau_1 = 57 \pm 5$ μs and $\tau_2 = 380 \pm 40$ μs (marked by the vertical dashed lines in Figure 3A). The fits of individual experiments are represented by the solid lines in Figure 3A. The corresponding amplitudes A_1 and A_2 varied with the delay. This dependence is shown in Figure 4A. The amplitudes A_1 and A_2 for the short and long photoreversal time constants show, apart from the sign and scaling factor, the same dependence on delay at 340 and 450 nm. The four discrete sets of amplitudes (A_1 and A_2 at two wavelengths) were fitted simultaneously with a sum of three exponentials (solid lines in Figure 4A). The optimal fit was obtained with time constants of 410 μs, 1.3 ms, and 500 ms identified by dotted vertical lines. The first two time constants, 410 μs and 1.3 ms, are close together and to the eye do not appear to provide a good description of the rise and decay of the A_1 amplitudes. This is a consequence of the partial cancellation of the positive and negative amplitudes associated with these time constants. Since the number of delay values is small, the errors in these time constants are large. The absolute value $|A_1|$ rises with a time constant of 410 μs. $|A_1|$ then decreases (1.3 ms), and in parallel, as expected for a sequential reaction, the amplitude $|A_2|$ rises. The A_1 amplitudes do not decay to zero, however, but reach a constant value after about 5 ms.

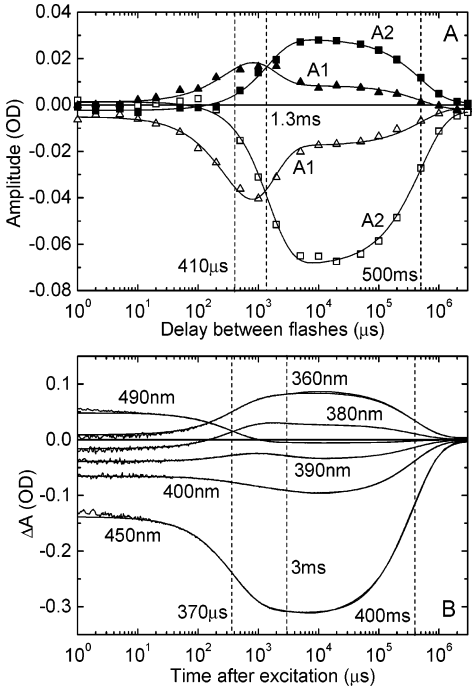

FIGURE 4: (A) Dependence of the amplitudes A_1 and A_2 on the delay. A_1 and A_2 are the amplitudes of the fast (57 μs) and slow (380 μs) photoreversal components, respectively. The two positive amplitudes with filled triangles (A_1) and squares (A_2) are at 340 nm; the two negative amplitudes with open triangles (A_1) and squares (A_2) are at 450 nm. The dashed vertical lines at 410 μs, 1.3 ms, and 500 ms indicate the values of the exponential time constants for a global fit with three exponentials. (B) Single flash (430 nm) absorbance changes for the same sample at 26 wavelengths varying from 330 to 510 nm. For clarity, only the traces at the indicated wavelengths are shown. The vertical dashed lines indicate the positions of the time constants for a global fit to all of the data with a sum of three exponentials; $\tau_1 = 370$ μs is the rise time of I_2, $\tau_2 = 3$ ms is the rise time of I_2', and $\tau_3 = 400$ ms is the decay time of I_2. The solid lines are the fits.

Finally, $|A_1|$ and $|A_2|$ decay together with a time constant of 500 ms. We note that the positive (340 nm) and negative (450 nm) amplitudes are to a very good approximation scaled mirror images.

Figure 4B shows for comparison the single flash (430 nm) kinetics at 6 selected wavelengths out of 26 collected from 330 to 510 nm. As we will show below, the I_2 and I_2' intermediates are in a thermal equilibrium after 3 ms. The model-dependent intermediate spectra for I_1 and the I_2/I_2' mixture, shown in Figure 1C, were calculated from these data in the following way. It was assumed that the cycle is sequential and unidirectional with only I_1 present at 10 μs and only the I_2/I_2' equilibrium mixture at 10 ms. Moreover, it was assumed that the I_2 and I_2' intermediates do not absorb at 446 nm. Using these assumptions, the spectrum of the I_2/I_2' equilibrium was determined by adding, to the difference spectrum at 10 ms [spectrum labeled (*) in Figure 6B, calculated from Figure 4B], a scaled amount of the ground-state spectrum to make the absorbance around 450 nm zero. The spectrum of I_1 was then calculated from the difference spectrum at 10 μs (from Figure 4B) by adding this same amount of the ground-state spectrum.

The complete 26-wavelength data set of Figure 4B was subjected to a global fit with three exponentials (solid lines). The three vertical dotted lines indicate the values of the three exponential time constants: 370 μs, 3 ms, and 400 ms. These

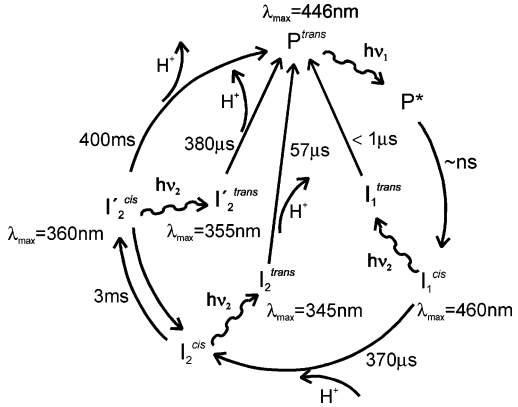

FIGURE 5: Proposed model for the PYP photocycle with sequential I_2^{cis} and $I_2'^{cis}$ intermediates which photoreverse to P^{trans} with exponential time constants of 57 and 380 μs, respectively (pH 6, 20 °C, 50 mM KCl). The photoreversal from $I_2'^{cis}$ may be slower than from I_2^{cis} since the global conformational change has to be reversed in addition to the other reset reactions. The short-lived intermediates I_0 and $I_0^{\ddagger}$ between P* and I_1 are not shown.

times correspond to the rise of I_2, the rise of I_2', and the return to the initial dark state. The presence of the 3 ms component (I_2 to I_2') can be clearly discerned in the data in Figure 4B (e.g., in the 390 nm trace). The reasonable agreement between these three time constants for I_2 and I_2' (Figure 4B) and the corresponding three values of 410 μs, 1.3 ms, and 500 ms for A_1 and A_2 (in Figure 4A) together with the dependence of A_1 and A_2 on the delay suggest the following interpretation of the photoreversal kinetics data in terms of a sequential model (Figure 5). The time constant of 57 μs is assigned to the photoreversal reaction from I_2 (I_2^{cis}). The very rapid photoisomerization from I_2^{cis} to I_2^{trans} is not resolved but leads to the initial positive absorbance change at 340 nm (see Figure 1A, difference between DFTV and BFTV at time zero and the positive spike at 10 ms in the DFTB trace). Between I_2^{trans} and P^{trans}, the chromophore deprotonates and returns to the binding pocket with a time constant of 57 μs. The time constant of 380 μs is assigned to the photoreversal reaction from I_2' ($I_2'^{cis}$). After the rapid unresolved photoisomerization to $I_2'^{trans}$, the chromophore has to be deprotonated and the global conformational change has to be reversed. In the sequential model, the delay dependence of A_1 and A_2 should reflect the time courses of the concentrations of I_2 and I_2', respectively. In agreement with this model, A_1 dominates at small delays, and A_2 rises concomitantly with the first decay phase of A_1. The rise time of A_1 (410 μs) agrees well with the rise time of I_2 (370 μs). The rise time of A_2 and the decay time of A_1 (1.3 ms) is only slightly ahead of the rise time of I_2' (3 ms). The common decay time of A_1 and A_2 (500 ms) agrees well with the decay time of I_2' (400 ms). In these respects, the unidirectional sequential model provides a good description for the observations and is summarized in Figure 5. On the other hand, if the transition between I_2 and I_2' were unidirectional, the amplitude of A_1 should go to zero in the 1.3 ms decay. This is, however, clearly not the case. The fact that A_1 remains constant after 5 ms at approximately 50% of its maximal value and finally decays to zero in a second decay phase (500 ms) together with A_2 is direct evidence for the existence of an equilibrium between I_2 and I_2'. I_2 and I_2' coexist after 5 ms and decay together. From the ratio of the A_1 and A_2 amplitudes around 10 ms (Figure 4A) we may

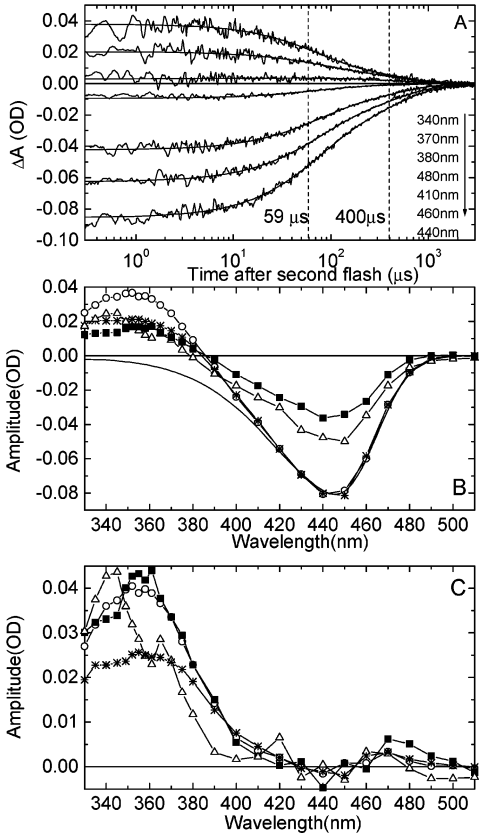

FIGURE 6: (A) Photoreversal signals at seven wavelengths between 330 and 510 nm at the fixed delay of 1 ms. For clarity, similar data at 19 additional wavelengths are not shown. The solid lines are the global fits with a sum of two exponentials with the common time constants $\tau_1 = 66$ μs and $\tau_2 = 413$ μs. A second data set (not shown) was acquired at a delay of 10 ms with global fit parameters $\tau_1 = 51$ μs and $\tau_2 = 391$ μs. The average τ's are marked by the vertical lines. (B) Amplitude spectra $A_1(\lambda)$ and $A_2(\lambda)$ associated with τ_1 and τ_2 obtained from the global fit of (A): (○) A_2 for the 10 ms delay; (■) A_2 for the 1 ms delay; (△) A_1 for the 1 ms delay. For comparison, the absorbance difference spectrum for the single flash experiment at 10 ms after the flash is shown (*, obtained from the data of Figure 4B). The A_2 spectrum at 10 ms (○) and the difference spectrum (*) are scaled at 450 nm to the spectrum of the dark state P (solid line). (C) Absorption spectra of $I_2'^{cis}$ (*), $I_2'^{trans}$ (○ at 10 ms delay, ■ at 1 ms delay), and I_2^{trans} (△) calculated from (B).

estimate that the I_2/I_2' equilibrium is on the side of I_2' with about 20−25% in I_2. The spectrum of the I_2/I_2' equilibrium in Figure 1C is thus mainly that of I_2'. The amplitude data clearly suggest a thermal back-reaction from I_2' to I_2. Thus, protein rearrangement must be faster than decay of I_2' and I_2 (500 ms), perhaps as fast as 400 μs.

Wavelength Dependence at the Fixed Delays of 1 and 10 ms. The wavelength dependence of the photoreversal signal was investigated at delays of 1 and 10 ms. At a delay of 1 ms A_1 and A_2 have comparable magnitude, whereas at a delay of 10 ms A_2 dominates (see Figure 4A). Data were collected at 26 wavelengths from 330 to 510 nm. The photoreversal signals were constructed as described earlier (see panels A and B of Figure 1 for examples at 340 and 450 nm at a 10 ms delay). Typical data for the delay of 1 ms and at seven selected wavelengths are displayed in Figure 6A together with their global two-exponential fits. The two common exponential time constants for this independent data set (at 26 wavelengths), at a delay of 1 ms, were 66 ± 5 and 410 ± 40 μs. For the data set at the delay of 10 ms (data not

shown), the two time constants were 51 and 390 μs. The rounded average values of 59 and 400 μs are marked by the dotted vertical lines (Figure 6A) and are in excellent agreement with the values of 57 and 380 μs determined from the delay data at the two wavelengths 340 and 450 nm (Figure 3A). The amplitude spectra A_2 (○ at 10 ms delay, ■ at 1 ms delay) and A_1 (△ at 1 ms delay) are plotted in Figure 6B together with the single flash difference spectrum at 10 ms (*) and the inverted ground-state spectrum (solid line).

Recall that the f_1 and f_2 corrections removed all contributions of the normal photocycle from the double flash signal. The photoreversal signal (PR) thus represents only the absorbance change due to photoreversal. In the previous section on the delay dependence, we argued that a sequential model provides a good description of the photoreversal kinetics: I_2^{cis} is photoreversed with the single decay time τ_1 and $I_2'^{cis}$ with the longer single decay time τ_2. We detected no further intermediates between I_2^{trans} and P nor between $I_2'^{trans}$ and P. The corresponding amplitude spectra $A_1(\lambda)$ and $A_2(\lambda)$ for such a two-state sequential model (I_2^{trans} to P and $I_2'^{trans}$ to P) are then equal to the difference spectra between the two states (I_2^{trans}/P and $I_2'^{trans}$/P, respectively). The spectra of I_2^{trans} and $I_2'^{trans}$ may thus be constructed from the A_1 and A_2 amplitude spectra in a simple way. This is illustrated for the A_2 amplitude spectrum at 10 ms in Figure 6B,C. First A_2 is scaled in such a way that it matches the inverted ground-state spectrum (P) at 450 nm (○). Figure 6B shows that the fit of the scaled A_2 spectrum to P is quite good in the wavelength range from 410 to 510 nm. This supports the assumption that, at least in this wavelength range, no states other than P contribute. By adding the ground-state spectrum to the scaled A_2 spectrum, the absorbance in the 410−510 nm range is now reduced to zero and the $I_2'^{trans}$ spectrum is generated (○ in Figure 6C). The same procedure was applied to the $A_2(\lambda)$ amplitude spectrum at 1 ms (■ in Figure 6B,C). The corresponding $I_2'^{trans}$ spectrum is within experimental error the same as that derived from A_2 at 10 ms, as it should be. In the same way the I_2^{trans} spectrum (△) was generated from the $A_1(\lambda)$ amplitude spectrum. In agreement with the observation of an instantaneous absorbance increase around 350 nm after the second flash (arrow in Figure 1A), the I_2^{trans} and $I_2'^{trans}$ intermediates have considerably higher extinction coefficients than I_2^{cis} (Figure 6C). Note that the extinction coefficient is not exactly zero above 410 nm but assumes small positive or negative values. This is due to experimental error in the determination of A_1 and A_2 at individual wavelengths. These errors are of the same magnitude as the differences between the two spectra for the $I_2'^{trans}$ intermediate derived from A_2 at 10 and 1 ms in the UV region.

At first sight, the spectrum for I_2^{trans} (△) appears to be anomalous due to the minimum at 361 nm. We recall that A_1, from which this spectrum is derived, is the amplitude of the fastest photoreversal component and therefore more affected by the flash. The absorption traces at the five wavelengths 349, 353, 355, 358, and 361 nm, closest to the excitation wavelength of 355 nm, are most affected by the flash artifact which leads to an artificially lower absorbance at these five wavelengths. Leaving these five wavelength traces out of the data analysis leads to the same absorbance at the wavelengths at or below 345 nm and at wavelengths at or above 365 nm. We conclude that the apparent minimum at 361 nm is due to the flash artifact. We may therefore conclude that the spectrum of I_2^{trans} is blue shifted with respect to the spectrum of $I_2'^{trans}$ by ~10 nm but has approximately the same maximal extinction coefficient. This blue shift is also apparent from the data points above 365 nm in Figure 6C, which are not affected by the flash artifact. From these spectra we estimate λ_{max} values of approximately 345 and 355 nm for I_2^{trans} and $I_2'^{trans}$, respectively.

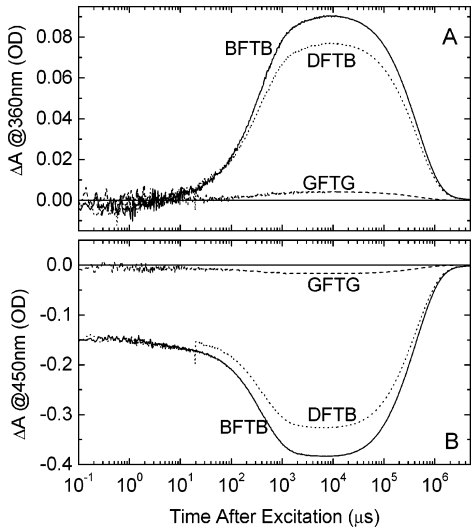

FIGURE 7: Photoreversal from I_1. The first flash (at 430 nm) was followed after 20 μs by a second flash (at 500 nm). Conditions: pH 6, 20 °C, 20 mM Tris, and 50 mM KCl. (A) Absorbance change at 360 nm. The trace labeled BFTB is the response after a blue single flash. DFTB labels the double flash response triggered on the first, blue flash. The trace labeled GFTG is the response after a single green flash. (B) Absorbance change at 450 nm. The meaning of the labels is as in (A). The positive unresolved absorbance change at 20 μs is due to about 18% photoreversal from I_1 to the initial dark state P.

Photoreversal from I_1. From the spectrum of I_1 in Figure 1C, it is clear that selective photoreversal from I_1 should be feasible with a second flash around 500 nm. Figure 7 shows double flash data at measuring wavelengths of 360 and 450 nm with a first flash, at 430 nm (blue), followed by a second flash, at 500 nm (green), after a delay of 20 μs. As expected, the green flash alone (GFTG) leads to very small effects due to the low absorbance of P at 500 nm. The photoreversal effect from I_1 can be most clearly discerned in the depletion signal (Figure 7B, 450 nm), since at this wavelength both I_1 and the initial dark state P absorb strongly, with the extinction coefficient of P being much larger than that of I_1 at this wavelength (Figure 1C). At 20 μs, a large positive absorbance change is observed (DFTB; the negative spike is the flash artifact), corresponding to the I_1 to P transition. This instantaneous positive absorbance step is not resolved when triggering on the first flash (DFTB). Triggering on the second flash (DFTG, not shown) also did not resolve this absorbance change. Thus, we can only conclude that photoreversal from I_1 is faster than 1 μs. At 20 μs, almost all molecules cycling are in I_1. The reduction in the number of cycling molecules at 20 μs by the 500 nm flash leads to a corresponding reduction in the amplitude of the depletion signal at 10 ms, since fewer I_2 molecules are formed. In Figure 7A (360 nm), no absorbance change is observed at 20 μs (apart from the negative spike), since the extinction coefficients of I_1 and P are quite small and similar at this wavelength (see Figure

1C). At 10 ms after the flash, the double flash amplitude (DFTB) is reduced by ~18% with respect to the single flash amplitude (BFTB). This reduction factor is the same as for the depletion signal at 10 ms and is due to the reduction in the population of I_2 caused by the photoreversal of the preceding intermediate I_1. Additional experiments were carried out at delays of 300 ns, 10 μs, and 10 ms (data not shown). At 300 ns and 10 μs, the amplitude of the photoreversal signal from I_1 was about the same as at 20 μs. This is as expected since I_1 has a rise time of about 3 ns and decays to I_2 in 300 μs. At a delay of 10 ms, photoreversal from I_1 could not be detected, since, at this delay, I_1 has decayed completely.

DISCUSSION

Using double flash excitation with a variable time delay between the blue (430 nm) and violet (355 nm) flashes, we investigated the kinetics of the photoreversal from the I_2^{cis} and $I_2'^{cis}$ intermediates to the initial dark state P. Figure 5 summarizes key aspects of the PYP photocycle and the integration of photoreversal processes into the overall photocycle. Photoisomerization to the I_2^{trans} and $I_2'^{trans}$ intermediates is the first step in photoreversal and is expected to be very rapid (on the order of a few picoseconds). We could not resolve these isomerization reactions, but we detected them by the instantaneous positive absorbance change in the 350 nm range immediately after the second flash (positive spike in trace DFTB and positive difference between traces DFTV and BFTV at time zero in Figure 1A). This initial *cis*−*trans* isomerization has been observed in previous single flash studies with a photo-steady-state mixture of I_2/I_2' and P but could not be resolved either (*24*). We note that our experiments do not provide definitive evidence that the initial unresolved absorbance is due to isomerization. This is the most likely explanation, however. In all photoreceptors studied to date, photoisomerization occurred in the excited state and was the first event after excitation. Femtosecond IR spectroscopy is the appropriate method to time-resolve the light-induced isomerization using suitable marker bands. Such experiments will be performed in the future.

Using a logarithmic time base and triggering on the second flash, we could time-resolve the slower dark phases of the photoreversal kinetics of I_2 and I_2'. From the data analysis of photoreversal signals, we obtained two exponential kinetic processes with time constants $\tau_1 = 57$ μs and $\tau_2 = 380$ μs (from the delay dependence) and $\tau_1 = 59$ μs and $\tau_2 = 400$ μs (from the wavelength dependence), which can be attributed to the dark phases of the photoreversal reactions of the I_2 and I_2' intermediates, respectively. In a sequential model, the delay dependence of the amplitudes A_1 and A_2, for the dark phases of the photoreversal reactions, should then reflect the time course of the I_2 and I_2' populations. Comparison of the corresponding time constants showed good agreement, except possibly for the rise of A_2 (1.3 versus 3 ms for the rise of I_2'). An exact agreement is not to be expected in view of the large errors in the time constants for the delay dependence of A_1 and A_2. This is due to the limited number of delay times (21 delay times between 1 μs and 3 s; see Figure 4A). Fitting these few data points over six decades of time with three exponentials necessarily leads to considerable errors. The fact that A_2 rises simultaneously with the decay of A_1 provides strong evidence for the sequential model.

In a unidirectional sequential model, the A_1 amplitude should decay to zero in parallel with the rise of A_2. Instead, A_1 drops to only about 50% of its maximal value around 5 ms, remains constant, and finally decays together with A_2 to zero in 500 ms. This suggests the presence of a thermal back-reaction from I_2' to I_2 and the corresponding existence of an I_2/I_2' equilibrium (Figure 5). Since chemical reactions are generally reversible, a strictly unidirectional photocycle is unlikely to be correct. In fact, we recently presented evidence for a pH-dependent equilibrium between the I_1 and I_2 intermediates in wild type and in the mutant E46Q (*20*).

The photoreversal method provides a powerful tool to prove directly the existence of thermal back-reactions. Suppose the intermediate I_n is photoreversed and the delay is set such that both the I_n and I_{n+1} states are populated. The second flash, which selectively excites I_n, leads to an instantaneous decrease in the concentration of I_n. If a back-reaction with I_{n+1} exists, the concentration of I_n will increase again by chemical relaxation of the I_n/I_{n+1} equilibrium. This allows a determination of the rate of the back-reaction. This idea was successfully applied to the equilibrium between the M and N intermediates of bacteriorhodopsin using the photoreversal from M (*28*) and should find application to PYP as well. Since the absorption spectra of I_2 and I_2' are very similar, the 355 nm flash used here cannot perturb the postulated I_2/I_2' equilibrium. Application to the I_1/I_2 equilibrium is more promising since these intermediates have very different absorption spectra, allowing selective excitation.

Comparing the spectra I_2^{trans} and $I_2'^{trans}$ in Figure 6C with that of the $I_2^{cis}/I_2'^{cis}$ equilibrium mixture, we conclude that the extinction coefficient of I_2' is much higher in the *trans* than in the *cis* form. This result confirms the experimental observation of Figure 1A that, at 340 nm (and neighboring UV wavelengths), there is a large instantaneous and unresolved increase in absorbance due to the *cis*−*trans* isomerization (difference between DFTV and BFTV traces at 1 μs). The origin of this difference in oscillator strength between the *trans* and *cis* forms of the protonated chromophore is not well understood, but the effect is large and seems to be common. For example, in the mutant E46Q, the dark *trans* form of the chromophore also has a much larger extinction coefficient around 350 nm than the I_2^{cis} form in the normal photocycle (*20*).

The absorption spectra of I_2^{cis} and $I_2'^{cis}$ differ somewhat, as is evident from the absorption changes in the time traces at 390 and 380 nm around 3 ms (the rise time of $I_2'^{cis}$) in Figure 4B. Our analysis of the A_1 and A_2 amplitude spectra, resulting in intermediate spectra of I_2^{trans} and $I_2'^{trans}$ of Figure 6C, shows that these spectra also differ. The spectrum of I_2^{trans} is blue shifted with respect to that of $I_2'^{trans}$ by roughly 10 nm. These observations are consistent with the view that the chromophore environment differs in the I_2 and I_2' states.

The dark phase of photoreversal, involving chromophore deprotonation, movement of chromophore back into the binding pocket, and reversal of global conformational change, is quite rapid: ~58 μs for I_2 and ~400 μs for I_2'. Moreover, these reversals occur in a single concerted step. The difference in the photoreversal kinetics of these two I_2 intermediates is a consequence of the different structure of

the two states. Reversal from I_2 involves chromophore deprotonation and a coupled movement of the chromophore back into the binding pocket and is thus rapid (58 μs). In the reversal from I_2', the global conformational change has to be reversed as well, leading to slower kinetics. Our data thus provide a first estimate of about 400 μs for the time constant of the protein refolding reaction. In the thermal decay of I_2 which occurs in a few hundred milliseconds, the isomerization is rate-limiting, and the reaction appears to occur with a single time constant.

We note that our sequential model is not unique and that other kinetic models could be used to explain our data. One such possibility is a nonsequential model with $I_2 \leftrightarrow I_2'$ being a dead-end side reaction from I_2; however, given the current understanding of the PYP photocycle and structure, Figure 5 represents the simplest working hypothesis.

I_2 and I_2' are difficult to distinguish with electronic absorption spectroscopy since their spectra are similar. Nevertheless, small but distinct effects are apparent in the transient absorption kinetics around 3 ms at selected wavelengths such as 390 nm [Figure 4B (*19*, *20*)]. The most convincing evidence for the existence of different I_2 intermediates (protonated chromophore) comes from time-resolved FTIR measurements (*17*, *18*). I_2 and I_2' can also be distinguished by the ability of I_2' to bind dyes (*19*, *21*) when a hydrophobic surface patch is exposed as a result of the conformational change (*22*). Here we showed that I_2 and I_2' can be differentiated kinetically using the double flash method with variable time delay, which was applied here for the first time to PYP.

Using a second flash at 500 nm, we directly showed the photoreversal from I_1. This reaction is fast (<1 μs) and possibly faster than our time resolution of about 50 ns. It is not surprising that the photoreversal kinetics from I_1 are much faster than from I_2. In the earlier I_1 intermediate, the chromophore remains deprotonated with the hydroxyl of the chromophore hydrogen-bonded to E46 and Y42. Thus, only the isomerization around the $C_7{=}C_8$ double bond has to be photoreversed. In I_2 and I_2', the cycle has advanced much further: chromophore protonation, loss of hydrogen bonds, surface exposure of the chromophore, and global conformational change. All of this has to be reversed in addition.

In recent work on the M intermediate of the light-driven proton pump bacteriorhodopsin, we were able to demonstrate a similar kinetic heterogeneity of the M substates by photoreversal kinetics (*6*). In the photoreversal from M, reisomerization and chromophore protonation are involved. As was the case for the I_2 intermediate of PYP, two photoreversal time constants were observed in BR (100 and 600 ns), which could be assigned to two sequential M intermediates that differed in the protonation state of the proton release group (*6*, *29*).

In previous work (*24*) the photoreversal kinetics from I_2 were investigated with single flash (355 nm) experiments on a photostationary mixture of I_2, I_2', and P, with a low pH of 5.6 required to accumulate a high population of I_2/I_2' under steady illumination, thus limiting this method to the low pH range. The observed exponential time constant was 147 μs at 20 °C and represents the average value over the I_2 and I_2' populations in the initial photo-steady-state mixture under these conditions. Likewise, the observed spectrum of I_2^{trans} was a superposition of the spectra of I_2^{trans} and $I_2'^{trans}$. The efficient excitation of the remaining 30% in the ground state by the 355 nm flash was ignored (see trace VFTV in Figure 1). The value of 147 μs (measured at pH 5.6) lies between our value of 57 μs for I_2 and 380 μs for I_2' (measured at pH 6), as expected for an average value. For the mutant M100A, which has a lifetime for I_2 of ~18 min at pH 6, nearly 100% of the PYP molecules are accumulated in the I_2/I_2' equilibrium under steady illumination (*25*). Using single flash excitation, an exponential time constant for photoreversal of 231 μs was obtained, consistent with the results presented here. The fact that the wild-type and M100A photoreversal kinetics are similar is not surprising, since current thinking is that M100 catalyzes the reisomerization but does not affect other steps in the photocycle (*25*). Thus, photoreversal kinetics should be similar to wild type and is consistent with the above interpretation.

In future work with the double flash method, it will be of particular interest to investigate the pH dependence of the photoreversal and the kinetics of the associated proton release.

ACKNOWLEDGMENT

We thank Elsa Chen, Dr. Stefan Dickopf, and Ingrid Wallat for technical support.

REFERENCES

1. Dickopf, S., Mielke, T., and Heyn, M. P. (1998) Kinetics of the light-induced proton translocation associated with the pH-dependent formation of the metarhodopsin I/II equilibrium of bovine rhodopsin, *Biochemistry 37*, 16888−16897.
2. Kiselev, A., and Subramaniam, S. (1994) Activation and regeneration of rhodopsin in the insect visual cycle, *Science 266*, 1369−1373.
3. Kendrick, R. E., and Kronenberg, G. H. M. (1994) *Photomorphogenesis in Plants*, 2nd ed., Kluwer Academic, Dordrecht.
4. Montgomery, B. L., and Lagarias, J. C. (2002) Phytochrome ancestry: sensors of bilins and light, *Trends Plant Sci. 7*, 357−366.
5. Spudich, J. L., Zacks, D. N., and Bogomolni, R. A.(1995) Microbial sensory rhodopsins: photochemistry and function, *Isr. J. Chem. 35*, 495−514.
6. Dickopf, S., and Heyn, M. P. (1997) Evidence for the first phase of the reprotonation switch of bacteriorhodopsin from time-resolved photovoltage and flash photolysis experiments on the photoreversal of the M-intermediate, *Biophys. J. 73*, 3171−3181.
7. Jiang, Z. Y., Swem, L. R., Rushing, B. G., Devanathan, S., Tollin, G., and Bauer, C. E. (1999) Bacterial photoreceptor with similarity to photoactive yellow protein and plant phytochromes, *Science 285*, 406−409.
8. Cusanovich, M. A., and Meyer, T. E. (2003) Photoactive yellow protein: a prototypic PAS domain sensory protein and development of a common signaling mechanism, *Biochemistry 42*, 4759−4770.
9. Hellingwerf, K. J., Hendriks, J., and Gensch, T. (2003) Photoactive yellow protein, a new type of photoreceptor protein: will this "yellow lab" bring us where we want to go?, *J. Phys. Chem. A 107*, 1082−1094.
10. Kyndt, J. A., Meyer, T. E., and Cusanovich, M. A. (2004) Photoactive yellow protein, bacteriophytochrome and sensory rhodopsin in purple phototrophic bacteria, *Photochem. Photobiol. Sci. 3*, 519−530.
11. Taylor, B. L., and Zhulin, I. B. (1999) PAS domains: internal sensors of oxygen, redox potential, and light, *Microbiol. Mol. Biol. Rev. 63*, 479−506.
12. Taylor, B. L., Zhulin, I. B., and Johnson, M. S. (1999) Aerotaxis and other energy-sensing behavior in bacteria, *Annu. Rev. Microbiol. 53*, 103−128.
13. Borgstahl, G. E. O., Williams, D. R., and Getzoff, E. D. (1995) 1.4 Å structure of photoactive yellow protein, a cytosolic photoreceptor: unusual fold, active site and chromophore, *Biochemistry 34*, 6278−6287.

14. Getzoff, E. D., Gutwin, K. N., and Genick, U. K. (2003) Anticipatory active-site motions and chromophore distortion prime photoreceptor PYP for light activation, *Nat. Struct. Biol. 10*, 663−668.
15. Genick, U. K., Borgstahl, G. E., Ng, K., Ren, Z., Pradervand, C., Burke, P. M., Srajer, V., Teng, T. Y., Schildkamp, W., McRee, D. E., Moffat, K., and Getzoff, E. D. (1997) Structure of a protein photocycle intermediate by millisecond time-resolved crystallography, *Science 275*, 1471−1475.
16. Ren, Z., Perman, B., Srajer, V., Teng, T. Y., Pradervand, C., Bourgeois, D., Schotte, F., Ursby, T., Kort, R., Wulff, M., and Moffat, K. (2001) A molecular movie at 1.8 Å resolution displays the photocycle of photoactive yellow protein, a eubacterial blue-light receptor from nanoseconds to seconds, *Biochemistry 40*, 13788−13801.
17. Xie, A., Kelemen, L., Hendriks, J., White, B. J., Hellingwerf, K. J., and Hoff, W. D. (2001) Formation of a new buried charge drives a large-amplitude protein quake in photoreceptor activation, *Biochemistry 40*, 1510−1517.
18. Brudler, R., Rammelsberg, R., Woo, T. T., Getzoff, E. D., and Gerwert, K. (2001) Structure of the I_1 early intermediate of photoactive yellow protein by FTIR spectroscopy, *Nat. Struct. Biol. 8*, 265−270.
19. Borucki, B., Devanathan, S., Otto, H., Cusanovich, M. A., Tollin, G., and Heyn., M. P. (2002) Kinetics of proton uptake and dye binding by photoactive yellow protein in wild type and in the E46Q and E46A mutants, *Biochemistry 41*, 10026−10037.
20. Borucki, B., Otto, H., Joshi, C. P., Gasperi, C., Cusanovich, M. A., Devanathan, S., Tollin, G., and Heyn, M. P. (2003) pH dependence of the photocycle kinetics of the E46Q mutant of photoactive yellow protein: protonation equilibrium between the I_1 and I_2 intermediates, chromophore deprotonation by hydroxyl uptake, and protonation relaxation in the dark state, *Biochemistry 42*, 8780−8790.
21. Hendriks, J., Gensch, T., Hviid, L., van der Horst, M. A., Hellingwerf, K. J., and van Thor, J. J. (2002) Transient exposure of hydrophobic surface in the photoactive yellow protein monitored with Nile Red, *Biophys. J. 82*, 1632−1643.
22. Meyer, T. E., Tollin, G., Hazzard, J. H., and Cusanovich, M. A. (1989) Photoactive yellow protein from the purple phototropic bacterium, *Ectothiorhodospira halophila*: quantum yield of photobleaching and effects of temperature, alcohols, glycerol, and sucrose on kinetics of photobleaching and recovery, *Biophys. J. 56*, 559−564.
23. Miller, A., Leigeber, H., Hoff, W. D., and Hellingwerf, K. J. (1993) A light-dependent branching reaction in the photocycle of the yellow protein from *Ectothiorhodospira halophila*, *Biochim. Biophys. Acta 1141*, 190−196.
24. Hendriks, J., van Stokkum, I. H. M., and Hellingwerf, K. J. (1999) Kinetics of and intermediates in a photocycle branching reaction of the photoactive yellow protein from *Ectothiorhodospira halophila*, *FEBS Lett. 458*, 252−256.
25. Devanathan, S., Genick, U. K., Canestrelli, I. L., Meyer, T. E., Cusanovich, M. A., Getzoff, E. D., and Tollin, G. (1998) New insights into the photocycle of *Ectorhodospira halophila* photoactive yellow protein: photorecovery of the long-lived photobleached intermediate in the M100A mutant, *Biochemistry 37*, 11563−11568.
26. Borucki, B., Otto, H., and Heyn, M. P. (1999) Reorientation of the retinylidene chromophore in the K, L, and M intermediates of bacteriorhodopsin from time-resolved linear dichroism: resolving kinetically and spectrally overlapping intermediates of chromoproteins, *J. Phys. Chem. B 103*, 6371−6383.
27. Otto, H., Marti, T., Holz, M., Mogi, T., Lindau, M., Khorana, H. G., and Heyn, M. P. (1989) Aspartic acid-96 is the internal proton donor in the reprotonation of the Schiff base of bacteriorhodopsin, *Proc. Natl. Acad. Sci. U.S.A. 86*, 9228−9232.
28. Druckmann, S., Heyn, M. P., Lanyi, J. K., Ottolenghi, M., and Zimanyi, L. (1993) Thermal equilibrium between the M and N intermediates in the photocycle of bacteriorhodopsin, *Biophys. J. 65*, 1231−1234.
29. Druckmann, S., Friedman, N., Lanyi, J. K., Needleman, R., and Ottolenghi, M. (1992) The back photoreaction of the M intermediate in the photocycle of bacteriorhodopsin: mechanism and evidence for two M species, *Photochem. Photobiol. 56*, 1041−1047.

BI0481141